Catalysis Today 432 (2024) 114582

Contents lists available at ScienceDirect

Catalysis Today

journal homepage: www.elsevier.com/locate/cattod

Removal of clozapine from polluted waters via C_3N_4 based materials

Vasilios Sakkas [a], Claudio Medana [b], Federica Dal Bello [b], Lucia Ingaramo [c], Christoforos Chrimatopoulos [a], Maria Cristina Paganini [c], Paola Calza [c,*]

[a] Department of Chemistry, University of Ioannina, Laboratory of Analytical Chemistry, Ioannina 45110, Greece
[b] Department of Molecular Biotechnology and Health Science, University of Turin, Piazza Nizza 44, Torino 10126, Italy
[c] Department of ChemistryUniversity of Turin, Via P. Giuria 5/7, Torino 10125, Italy

ARTICLE INFO

Keywords:
Semiconductor heterojunction
Advanced oxidation processes
Natural waters
Clozapine

ABSTRACT

New photocatalysts with a g-C_3N_4-ZnO heterojunction were prepared following different synthetic routes, fully characterized, and evaluated for the abatement of the antipsychotic drug clozapine. Experiments were performed with clozapine standard and clozapine based commercial tablet solutions in a sun simulator and the evaluation of clozapine removal was assessed in different aqueous media: Milli-Q and natural water (Po River) to evaluate the role of natural occurring components on the drug removal efficiency. The photocatalyst prepared via hydrothermal method (CA_1) exhibited the highest efficiency, allowing to achieve the complete abatement of clozapine within 30 min, in Milli-Q water. Its photocatalytic performance decreased in river water, where the total drug degradation was obtained after1h, and is notably inhibited on Leponex tablets (80% removal after 1 h of irradiation). Clozapine degradation proceeds through the formation of nineteen (19) transformation products, all less hazardous that the parent compound, as proved by the acute and chronic toxicity valued by ECOSAR. Mechanistic studies evidenced that $OH^{\bullet}$ radicals are the key reactive species involved in the pollutant removal, while other species such as superoxide radical anion ($O_2^{\bullet-}$) and especially singlet oxygen (O_2^1) played a marginal role in the degradation process.

1. Introduction

The consumption of psychotropic drugs is increasing, especially in high-income countries, with their consequent significant release into the environment [1]. In particular, during the period of the COVID-19 pandemic, a growth in mental health issues was observed which had led to the rise in the use of antipsychotic drugs [2]. Pharmaceuticals, including antipsychotics, are a group of contaminants of emerging concern with the highest frequency of detection in wastewater, surface and ground water, and even drinking water [3,4], at concentration ranging from a few ng/L up to μg/L [5–7].

The scientific community has taken a keen interest in understanding the source, occurrence, and behaviour of these compounds in wastewater and receiving waters. They are released into the aquatic ecosystems by human metabolism followed by excretion, or by wastewater from hospitals and pharmaceutical industries ending up to WWTPs [7,8] with quite low removal efficiencies [4].

The fate of antipsychotics, once released into surface water, is unpredictable. Hydrolysis, photolysis or biodegradation are processes that may contribute to pollutant degradation [9,10], but in most of the cases these drugs show a high stability. These substances, when released into aquatic ecosystems, can undergo transformation promoted by sunlight [11–13]. Processes in which organic pollutants directly absorb photons from sunlight (direct photolysis), or reactive species generated by the photolysis of other compounds in water, such as dissolved organic matter (indirect photolysis), can contribute to the degradation of psychiatric drugs from surface waters [6], and transformation products may be formed, with different and even more hazardous properties than the parent compound [14].

Therefore, the complete removal of these drugs from water bodies is challenging due to their persistence and complex chemical structures [15]. In recent years, the photocatalytic process has emerged as a promising method for the removal of psychiatric drugs from water [16]. Under proper irradiation, several reactive species, such as hydroxyl radicals or superoxide radicals [17], are generated and exploited to efficiently degrade psychiatric drugs and their by-products, resulting in their mineralization to harmless end products [18,19]. Indeed, a previously reported study investigated the photocatalytic behaviour of

* Corresponding author.
E-mail address: paola.calza@unito.it (P. Calza).

https://doi.org/10.1016/j.cattod.2024.114582
Received 24 October 2023; Received in revised form 23 January 2024; Accepted 8 February 2024
Available online 14 February 2024

Table 1
Labels and synthesis details for all the photocatalysts and their energy band gap (eV) calculated via Tauc Plot method.

Sample name	Synthesis details	Eg (eV)
ZnO_H	$Zn(NO_3)_2 \times 6\ H_2O$ –> autoclave (175°C, 16 h) –> oven (70°C, 12 h)	3.30
US 2:1	ZnO_H + g-C_3N_4 [ratio 2:1] –> ultrasound (30 min) –> oven (70°C, overnight)	3.15
US 3:1	ZnO_H + g-C_3N_4 [ratio 3:1] –> ultrasound (30 min) –> oven (70°C, overnight)	3.22
CA_1	$Zn(NO_3)_2 \times 6\ H_2O$ + Melamine –> autoclave (175°C, 12 h) –> oven (70°C, 12 h) –> calcined at 550°C for 4 h, 10 °C/min	2.85
DEP 1:1	ZnO_H + Melamine [ratio 1:1] –> oven (70°C, 2 days) –> calcined at 550°C for 4 h, 10 °C/min	3.20
DEP 2:1	ZnO_H + Melamine [ratio 2:1] –> oven (70°C, 2 days) –> calcined at 550°C for 4 h, 10 °C/min	3.21
DEP 3:1	ZnO_H + Melamine [ratio 3:1] –> oven (70°C, 2 days) –> calcined at 550°C for 4 h, 10 °C/min	3.22

clozapine utilizing the benchmark TiO_2as photocatalyst [20].

However, optimizing photocatalyst materials is a challenging process. Zinc oxide (ZnO) has also been extensively studied for its many excellent properties [21]. Nevertheless, certain obstacles such as chemical or photo-corrosion mechanisms need to be addressed to enhance the photocatalytic efficiency. In this context, the combination of ZnO with other semiconductors emerges as a favourable and promising alternative. Semiconductor heterojunctions present intriguing approaches in creating highly efficient photocatalysts. One of these materials is graphitic carbon nitride, g-C_3N_4, which is an organic semiconductor that has been extensively investigated in photocatalytic applications due to its favourable stability and band gap of 2.7 eV [22,23]. The coupling of g-C_3N_4 with ZnO in a heterojunction structure is supposed to offer several advantages. First, it can help to stabilize the ZnO material, thereby mitigating the issue of photo-corrosion. Second, the heterojunction interface between g-C_3N_4 and ZnO can promote efficient charge separation and transfer, enhancing the overall photocatalytic activity. Third, this combination can lead to a better absorption of solar radiation, thus extending the photocatalytic response to the visible light spectrum, making the catalyst more effective under solar irradiation. Moreover, the advancement of simple, effective, and economical techniques for synthesizing heterostructures with strong stability and photocatalytic properties, particularly under visible-light or solar irradiation, can significantly contribute to promoting the widespread application of heterogeneous photocatalysis on a large scale.

Given that, clozapine exhibits significant stability during wastewater treatment plant (WWTP) removal processes, with a removal efficiency ranging from negative values up to 49% [15]; this research sought to create new materials capable to improve its removal. For this purpose, seven distinct g-C_3N_4-ZnO composite materials were developed and their photocatalytic performance and mechanism in degrading clozapine in different water matrices was assessed. Our work introduces a novel approach by synthesizing advanced g-C_3N_4-ZnO photocatalysts from diverse precursors, emphasizing thorough characterization to assess their effectiveness in the photocatalytic degradation of clozapine, a remarkably stable compound found in wastewater. Notably, our study goes beyond conventional testing in pure aqueous solutions, extending to evaluations in natural waters and commercial tablets. A key focus is the identification of transformation products, facilitated by LC-HRMS and the degradation pathways involved. Toxicity assessments were also carried out employing the US EPA ECOSAR computer model, contributing significant insights to the field.

2. Materials and methods

2.1. Reactants

Leponex® tablet (Novartis, Germany) inclosing 25 mg clozapine and several excipients (48 mg of lactose monohydrate, maize starch, talc, magnesium stearate, colloidal anhydrous silica and povidone (K30)) was dissolved in ultrapure water, daily, and the solution was stored in the dark before use. Ultrapure water was produced by a Milli-Q system (Evoqua, Pittsburg, USA). To perform the scavenger studies, isopropyl alcohol was purchased from Fisher Chemical (Pittsburgh, Pennsylvania, USA), while p-benzoquinone and sodium azide were purchased from Sigma-Aldrich (Athens, Greece).

All the organic and inorganic reagents employed in the synthesis of the materials were purchased from Sigma-Aldrich and used without any further purification procedure. The different materials prepared in this work, the precursors employed, and the synthetic route involved are summarized in Table 1 (*vide infra*).

2.2. Synthesis procedures

Pristine zinc oxide was synthesized using the hydrothermal method described in a previous work [24]. Briefly, an aqueous solution of 1 M Zn $(NO_3)_2$ was prepared and, when the zinc salt was completely dissolved, a 4 M NaOH solution was slowly added dropwise to the initial solution until a pH 11–12 was reached and a dense white precipitate, $Zn(OH)_2$, was formed. The precipitate was then put in a stainless-steel autoclave and heated at 175°C for 16 h. The resulting ZnO, labelled ZnO_H was then rinsed with water, collected through centrifugation, and dried at 70°C overnight.

Then, heterostructered systems were prepared by mixing bare ZnO and melamine at different ratios following three different synthetic routes. All the syntheses details and the acronyms are summarized in Table 1, while details on C_3N_4 synthesis are reported in supplementary material.

ZnO_H was mixed with two different stoichiometric ratios of g-C_3N_4 previously obtained by heating melamine under atmospheric conditions. The powders were dissolved in water and the mixed systems were kept under ultrasound sonication for 30 min. The samples obtained were labelled US 2:1 and US 3:1. This method aimed to achieve exfoliation of C_3N_4 sheets for deposition onto the surface of ZnO. Again, considering the effective dispersion of the starting materials, water was employed as a suitable medium to achieve a homogeneous suspension. The bulky starting materials, ZnO and C_3N_4, obtained by hydrothermal synthesis and melamine condensation, respectively, were utilized for the mechanical mixing process.

The sample named CA_1 was prepared *via* hydrothermal synthesis starting from mixing the basic precursors $Zn(NO_3)_2$ and melamine. The samples named DEP were prepared mixing ZnO_H and melamine with different ratios (1:1, 2:1 and 3:1) and calcined at 550°C (see Table 1).

2.3. Characterization techniques

X-ray powder diffraction (XRPD) was utilized to gather structural information about the synthesized materials, both single and multiple phases. Particular attention was paid to phase identification and the possible presence of impurity reflections, especially originating from the organic precursors. The patterns were acquired using a PANalytical PW3040/60 X'Pert PRO MPD instrument in a Bragg-Brentano geometry, with a copper K radiation source (0.15418 nm), operated at 45 kV and 40 mA. The scanning range for 2θ was between 10° and 80°. Mineral phases in the samples were identified using the X'Pert High-Score software (Malvern Panalytical Ltd, Malvern, UK).

Diffuse Reflectance UV-Vis spectroscopy was employed to characterize the samples optically. Optical spectra were recorded using a Varian Cary 5000 spectrophotometer (Agilent, CA, USA) with the

Carywin-UV/scan software (Agilent, CA, USA). A sample of PTFE with 100% reflectance was used as the reference. The optical band gap energies were calculated using the Tauc plot method on the obtained spectra. The energy gap is proportional to the absorption coefficient near the absorption edge, and its value depends on the type of transition (direct or indirect allowed) [25].

The Field Emission Scanning Electron Microscope (FESEM) images were taken with the FEG-SEM TESCAN S9000G instrument. The microscope features a Schottky emitter as the electron source, providing a resolution of 0.7 nm at 15 keV (In-beam SE). The accelerating voltage can be adjusted from 0.2 to 30 keV. The microanalysis system used is OX-FORD - detector Ultim Max - software AZTEC.

2.4. Irradiation procedures

2.4.1. Photocatalytic process

Experiments were performed to investigate the degradation of clozapine in water using seven different g-C_3N_4-ZnO based materials. The tests were executed both on the aqueous standard of clozapine and on the 25 mg tablet of Leponex. The catalysts powders were dissolved in MilliQ water, and the mixed systems were kept under ultrasound sonication using the Sono plus instrument by Bandelin Sonicator. A solution of clozapine (10 mg/L) with the addition of each catalyst (100 mg/L) was prepared and exposed to simulated solar conditions using a Suntest CPS+ apparatus (Heraeus; Hanau, Germany). The lamp used had a power of 1500 W, which was adjusted to 750 W/m^2 to simulate solar emission in the range of 300–800 nm. A glass filter was employed to prevent transmission of wavelengths below 290 nm.

The clozapine/catalyst solution (50 mL) was placed in a Pyrex glass reactor, tightly sealed to avoid liquid evaporation, and magnetic stirring was employed during irradiation (see scheme S1 in supplementary material). A tap-water cooling system was used to maintain the temperature below 25°C. Samples were withdrawn from the reactor at specific time intervals. After the irradiation process, the samples were centrifugated at 10,000 rpm to remove the suspended catalyst and subjected to analysis using an HPLC–UV-Vis DAD equipment. The degradation kinetics of clozapine were determined by analysing the concentration versus time curves. The data were fitted to a pseudo-first order equation ($C_t = C_0\, e^{-kt}$) in all cases to calculate the respective rate constants (k).

The photodegradation experiments aimed to studying the transformation of the molecule were performed in Pyrex glass cells equipped with a side neck and screw cap on 5 mL solution containing 10 mg/L of clozapine and 100 mg/L of catalyst. The cells were placed under a 1500 W xenon lamp (Solarbox, CO.FO.ME.GRA., Milan, Italy) with a filter for 340 nm radiation. After the pre-established irradiation time, the solution was filtered through a 0.45 μm filter (Millipore Millex-LCR, hydrophilic PTFE) and analysed.

Po River water was sampled on 20 June 2022 in Turin, (Valentino Park) and the sampling point was chosen as close as possible to the middle of the mainstream from the surface water layer, i.e. 0–5 cm from the surface. The sampled water was kept in amber glass bottles equipped with Teflon-coated screw caps, filtered with 0.7 μm GF-F glass fiber filters (Whatman) and stored in a refrigerator. The main water parameters were determined and are collected in Table S1 in supplementary material.

2.4.2. Scavenger studies

To investigate the mechanisms by which the synthesized catalysts degrade clozapine, additional scavenger studies were performed. Different solutions of clozapine (standard and tablet) at 10 mg/L and catalyst (100 mg/L) were prepared and irradiated (Suntest), with different additions of isopropyl alcohol (1 M), benzoquinone (1 mM), and sodium azide (5 mM). The irradiation conditions were the same as described above (Section 2.3.1). To assess the mechanism of each catalyst, the rate constant (k) was calculated and compared with the initial values, without the scavenger addition.

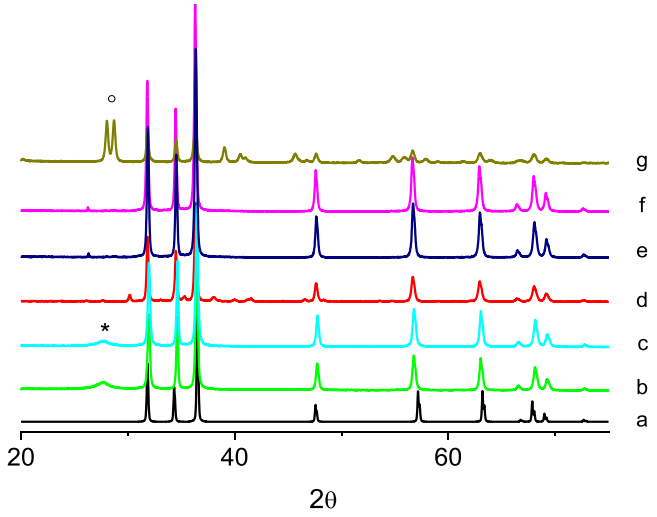

Fig. 1. XRPD pattern of the synthesized samples: a) ZnO_H, b) US 2:1, c) US 3:1, d) CA_1, e) DEP 3:1, f) DEP 2:1, g) DEP 1:1, * is referred to the presence of C_3N_4 species, ° is related to unreacted precursors.

2.5. Analytical techniques

The kinetics of clozapine were monitored using a HPLC UltiMate 3000 coupled with UV-Vis - Diode Array Detector (HPLC–UV/Vis DAD) (Thermo Scientific, Waltham, Massachusetts, USA). A 20 μL injection volume was introduced into the chromatographic system for the analysis. The analytical column used was a 150 × 4.6 mm Hypersil GOLD column, with a particle size of 5 μm (Thermo Scientific, Waltham, Massachusetts, USA). The column was maintained at a temperature of 25°C. The chromatographic conditions were identical with a previously reported gradient program [6], while the entire chromatographic analysis was completed within 15 minutes. The DAD of the system was set to monitor clozapine at a wavelength of 230 nm [5], with full spectra scanning from 200 to 400 nm. Mobile phase consisted by a mixture of methanol and ortho-phosphoric acid (0.3%) at a flow rate of 1 mL/min.

High performance liquid chromatography (HPLC) coupled to high resolution mass spectrometry (HRMS) was used to analyse the transformation products. A Thermo Scientific™ Dionex™ UltiMate™ 3000 Basic Automated System chromatograph coupled with a Thermo Scientific™ Orbitrap Fusion™ Tribrid™ high resolution mass analyzer via a H-ESI (Electrospray Ionisation) type ion source were used. A C18 Phenomenex Luna® column 150 mm×2 mm was used, thermostated at 30°C. The method involved injection volume of 20 μL, a mobile phase composed of a mixture of acetonitrile and 0.1% formic acid in water and a flow rate of 0.200 mL/min.

2.6. Toxicity assessment

The acute toxicity of clozapine and its transformation products was evaluated for three organisms (fish, daphnid, green algae) using the ECOSAR software v2.2. Chronic toxicity concentrations for these organisms were also computed using the same software [26,27].

3. Results and discussion

3.1. Materials characterization

The XRPD patterns of the C_3N_4-ZnO heterojunction, formed by the different synthetic paths described in the above section and summarized in Table 1, are depicted in Fig. 1.

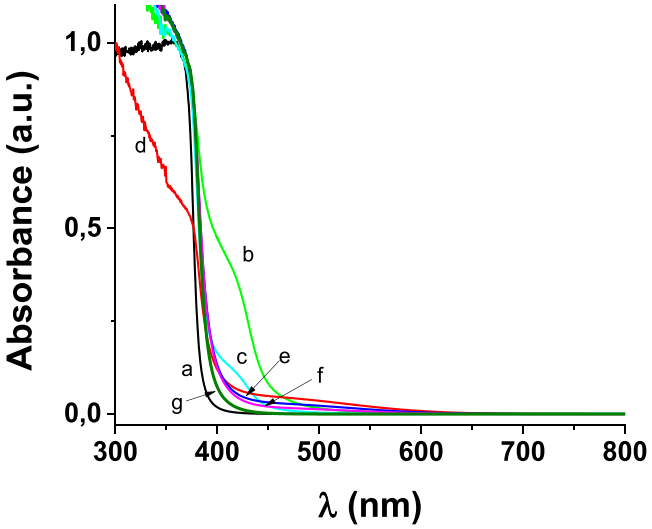

Fig. 2. DR-UV-Vis spectra of the synthesized samples: a) ZnO_H, b) US 2:1, c) US 3:1, d) CA_1, e) DEP 3:1, f) DEP 2:1, g) DEP 1:1.

It can be observed that the XRPD patterns of the prepared materials are primarily characterized by the typical reflections of ZnO. These reflections correspond to the (100), (002), (101), (102), (110), (103), (200), (112), (201), (004), and (104) planes, respectively, which are attributed to the typical wurtzitic hexagonal crystal phase (JCPDS 36–1451) [28]. The sharpness of these reflections confirms the purity and high crystallinity of the ZnO phase.

However, in the case of the CA_1 and DEP 1:1 samples, the intensity of the ZnO phase reflections is not as pronounced, and both samples show additional reflections due to impurities introduced by unreacted supramolecular reagents, in particular unreacted melamine. It is worth noting that no significant signals attributable to C_3N_4 were observed due to the low intensity of these reflections; only in the case of samples US 2:1 and US 3:1, it is possible to observe weak peaks attributed to C_3N_4 species.

By analyzing these patterns, an additional noteworthy characteristic emerges. The different relative intensity ratios of the three main reflections of the ZnO phases (within 2θ values of 30° and 40°) in the samples grown simultaneously with the carbon nitrate phase, compared to pristine ZnO, clearly indicate a certain preferential directional growth of ZnO in the presence of the additional phase. The nature of the precursor for the latter phase also influences this phenomenon, shaping the geometry and aspect ratio of the nanoparticles.

The absence of crystallographic peaks corresponding to C_3N_4 in the combined samples can be attributed to several factors. Firstly, the low atomic mass of carbon and nitrogen nuclei contributes to the limited detectability by XRD. Additionally, the formation of needle-like or thin sheet structures prevents the development of a periodic structure suitable for detection by XRD.

Interestingly, in contrast to other studies [29,30], the crystallinity of the ZnO phase is not compromised in the final heterojunction. The reflections corresponding to ZnO in the mixed materials retain the same high intensity and sharpness as those observed in pristine ZnO.

While XRPD analysis does not indicate the presence of C_3N_4, DRS UV-Vis spectroscopy reveals characteristic features attributed to the carbon nitride phase, as observed in Fig. 2. Generally, all the mixed C_3N_4-ZnO materials exhibit a different behaviour than the bare ZnO. This can be deduced from the calculated energy gap values obtained from the Tauc plot (Table 1) and show a slight red shift compared to ZnO's optical absorption. The enhanced absorption of visible photons in the case of the heterojunctions can be attributed to the presence of nitride, suggesting a strong cooperative effect between the two phases at the interface.

Furthermore, the presence of an absorption tail at about 500 nm, absent in the pristine ZnO sample, can be attributed to a higher level of defects in this phase within the mixed system. This is likely a result of the simultaneous crystallization of C_3N_4 with the ZnO phase during the C_3N_4 condensation process, as discussed in previous studies [29–31].

From an optical perspective, the three materials obtained *via* deposition method (DEP 1:1, 1:2 and 3:1) display a similar trend, with a slight red shift in the absorption edge compared to pristine ZnO and an absorption shoulder around 500 nm. Among these materials, DEP 3:1 exhibits a higher absorption tail in the visible region (around 500 nm, spectrum e), indicating a stronger cooperation between the oxide and nitride phases following the second calcination step. This highlights the importance of optimizing the reaction time in the deposition synthetic route, which is dependent on the quantity of the organic precursor. Achieving the desired performance in terms of visible light harvesting in the heterojunctions relies on identifying the optimal reaction time for the specific amount of the organic precursor.

The DRS UV-Vis spectra for the samples labelled as US 2:1 and 3:1 prove a negligible red-shift in the band gap, like previous observations, with the values remaining approximately 3.20 eV. Finally, the UV-Vis analysis for the sample CA_1 (spectrum d) highlights a red shift respect to the spectrum of bare ZnO, together with a larger absorption shoulder with a long tail observed until 600 nm; this material exhibits the longest extension of absorption shoulders. CA_1 sample has been prepared mixing both the precursors, zinc nitrate and melamine and, in this case, the two materials and the relate heterojunctions formed together at the same time.

FESEM measurements were performed to compare the three distinct kinds of samples, namely US, DEP and CA, in particular to verify the presence of carbon nitride on the surface of the bare ZnO (Fig. 3).

The three characterization techniques are complementary and can describe the complexity of the prepared materials according to the different kind of synthesis. In the case of the sample US, the presence of C_3N_4 is detected both by XRD and UV-Vis, but surprisingly it is not possible to observe any evidence of it in the FESEM images. In this case probably the phase C_3N_4 crystallized in bigger and very localized

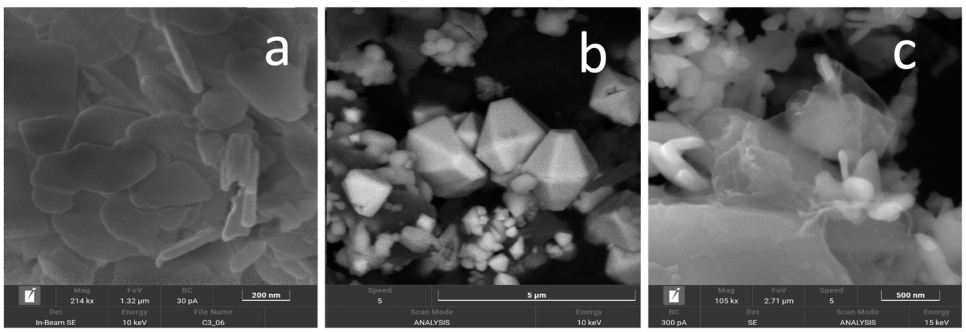

Fig. 3. FESEM images of the samples a) US 3:1, b) CA_1 and c) DEP 3:1.

Table 2
Kinetic constants and half-life for clozapine in Leponex tablet with all the developed materials.

	ZnO_H	US 2:1	US 3:1	CA_1	DEP 1:1	DEP 2:1	DEP 3:1
k (x100), min^{-1}	0.57 ±0.08	1.52 ±0.07	1.35 ±0.09	2.38 ±0.2	1.36 ±0.1	1.37 ±0.12	2.52 ±0.2
$t_{1/2}$ (min)	120.8	45.7	51.4	29.1	51.1	50.9	26.5

Table 3
Kinetic constants calculated in the presence of different scavengers.

	k, min^{-1} x 10^2	
Scavenger	**CA_1**	**DEP 3:1**
No scavenger	1.18±0.2	1.31±0.3
Isopropyl alcohol	2.00×10^{-2} ±0.01	1.00×10^{-2}±0.01
Benzoquinone	4.00×10^{-2} ±0.01	5.00×10^{-2} ±0.02
Sodium azide	0.29±0.04	0.61±0.05

crystals so it was possible to detect them via XRD, but they were not present in the region that was analyzed via FESEM. Ultrasound treatment has a significant impact on the morphology of ZnO particles, causing them to change dramatically from the typical hexagonal shape to flattened platelets. On the contrary, the sample CA presents a very well defined ZnO crystals, with high crystallinity, together with smaller crystals of unidentified shape. Also, in this case the existence of C_3N_4 was not detected by FESEM but its presence can be demonstrated by the long absorption shoulder in the UV-Vis spectra (spectrum d in Fig. 2). Finally, the sample DEP shows in FESEM images the clear presence of sheets of C_3N_4, these are so thin that are not detectable by XRD. In all cases EDX analysis has been also performed and, in all cases, the presence of C and N has been identified.

3.2. Photocatalytic testing of the materials

All the developed g-C_3N_4-ZnO based materials were assessed for the removal of clozapine dissolved in Milli-Q water; both the drug standard and the commercial tablet Leponex® were considered. To reach the adsorption equilibrium, clozapine and the catalysts were mixed and kept in the dark under magnetic stirring for 1 h. After the equilibration time, the adsorption of the drug is negligible for all the tested materials (see Table S2). The direct photolysis process was inspected for up to 24 h of irradiation and, in both cases, clozapine showed minimal photolysis (see Figure S2).

The disappearance of clozapine in Leponex® in the presence of the synthetized materials under irradiation follows a pseudo-first order decay and the calculated kinetic constants and half-life times are collected in Table 2, while the degradation profiles are shown in Figure S3.

The obtained results displayed that the most efficient catalysts are DEP 3:1 and CA_1. The former was synthesized by deposition with a lower ZnO/melamine stoichiometric ratio compared to the other two deposition-synthesized heterojunction systems. This could indicate that a high concentration of g-C_3N_4 dopant hinders charge separation, resulting in a slowing of the reaction kinetics. For the catalyst CA_1, prepared from zinc nitrate hexahydrate and pyrolyzed melamine, its efficiency could be attributed to the in-situ synthesis of g-C_3N_4. The characterization of these materials showed that the samples are crystalline, they present a pronounced or less pronounced absorption in the visible region and well-defined particles shape. The different synthesis procedures seem to poorly affect the activity of the two materials even if in one case the presence of g-C_3N_4 is clearly evidenced in the FESEM analysis and in the other case was not possible to detect it, only EDX outlined the presence of the carbon nitride.

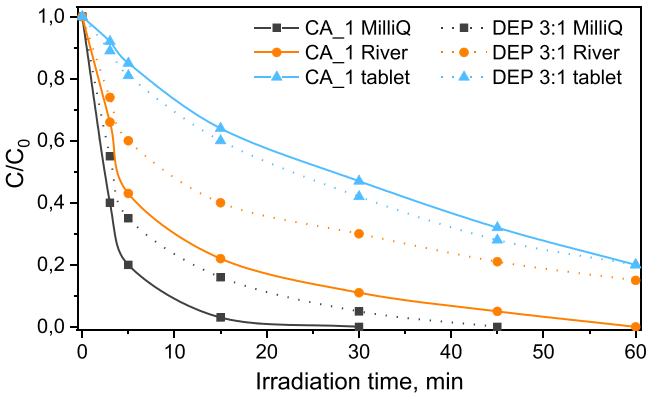

Fig. 4. Disappearance of the clozapine in MilliQ water, River water and Leponex tablet in the presence of CA_1 and DEP3:1.

In conclusion, DEP 3:1 and CA_1 photocatalysts were selected for a further investigation aimed to unravel the main photogenerated reactive species and to identify the transformation products formed during the pollutant abatement.

3.2.1. Effect of scavengers

The radical-quenching experiments were performed by using different scavengers aimed to qualitatively analyse the dominant active species, and results are shown in Table 3 and figure S4. Isopropyl alcohol (1 M), p-benzoquinone (1 mM) and sodium azide (NaN_3) 5 mM were used to inhibit the formation of hydroxyl radical (OH), superoxide anion radical (O_2^-) and singlet oxygen ($^1O_2$), respectively, based on reactions 1–3 [32]:

$$OH + (CH_3)_2CHOH \rightarrow H_2O + (CH_3)_2COH \quad (1)$$

$$BQ + O_2^- \rightarrow BQ_2^- + O_2 \quad (2)$$

$$N_3^- + {}^1O_2 \rightarrow N_3^{\cdot} + O_3^- \quad (3)$$

The kinetic constants acquired in these experiments are collected in Table 3, while the disappearance curves related to the two investigated catalyst (CA_1 and DEP 3:1) are plotted in Fig. S4.

It is clear the effect of the scavengers on the removal of the pollutant. The addition of isopropyl alcohol caused a strong decrease in the removal efficiency with a 130- and 60-folds decrease in the rate constant for DEP3:1 and CA_1, thus suggesting that OH radicals are the key reactive species involved in the removal of the pollutant. With the addition of benzoquinone, the rate constant decreases of around 30 times for both catalysts, so implying that the superoxide radical anion ($O_2^{\bullet-}$) is also playing a certain role. The addition of sodium azide induced only a slight inhibition in the abatement of pollutant (k decreased 4 and 2 times with DEP3:1 and CA_1, respectively), so entailing that singlet oxygen (O_2^1) played a marginal role in the degradation process.

3.3. Performance evaluation in natural waters

The applicability of the selected catalysts was also explored in natural water and on the commercial tablet by studying the drug removal in diverse matrices. Fig. 4 illustrates the degradation profiles of the photocatalyzed degradation followed by the antipsychotic drug in the different matrices. Relatively high photocatalytic rates were observed with both materials in Milli-Q water, whereas the performance of both catalysts is reduced when the process occurs in river water and on drug tablets.

Po River water was sampled as described in 2.4.1 and irradiated under a solar simulator in the presence of CA_1 and DEP 3:1. Analysing the results obtained in river water, the presence of dissolved organic

Table 4
Transformation products formed from clozapine through a photocatalytic process with CA_1 and DEP 3:1 in the MilliQ water and River water.

$[M+H]^+$	R_t (min)	CA_1 (Milli-Q)	CA_1 (River water)	DEP 3:1 (Milli-Q)	DEP 3:1 (River water)
219.1600	1.36	X	x	*n.d.*	*n.d.*
244.0638	8.84	X	x	*n.d.*	*n.d.*
245.1398	3.19	*n.d.*	*n.d.*	x	*n.d.*
293.1759	7.54	*n.d.*	*n.d.*	x	x
299.1500 A-B	2.87; 5.44	*n.d.*	*n.d.*	x	x
301.1213	8.87	X	x	x	x
309.1701	3.46	X	*n.d.*	x	x
313.1218	11.57	X	x	*n.d.*	*n.d.*
329.1163	11.26	*n.d.*	*n.d.*	x	x
341.1607 A	2.66	X	x	x	x
341.1607 B	4.03	*n.d.*	*n.d.*	x	*n.d.*
343.1321 (A-D)	8.57;11.36;11.57;12.13	X	x	x	x
345.1478	13.38	X	*n.d.*	*n.d.*	*n.d.*
359.1275 (A–B)	7.62–10.73	X	x	*n.d.*	*n.d.*

matter (DOM) and of inorganic anions, such as NO_3^-, Cl^-, HCO_3^- and CO_3^{2-}, could play a double role. On one side, a decrease in drug removal is expected and is well documented in literature [33,34], as the active species involved in the degradation of clozapine are competing with DOM and the photosensitivity of DOM could induce a decrease in the light flux, so hindering the absorption of light from the catalyst. On the other side, the components of natural water could contribute to the drug degradation thanks to indirect photolysis processes mediated by natural species, e.g. dissolved organic matter, nitrite and nitrate ions, H_2O_2 and iron species [35].

Overall, the two catalysts retain a good efficiency in the pollutant removal also in River water, and especially CA_1 demonstrated remarkable efficiency in removing the target molecule within one hour. At the same time, DEP 3:1 led to the removal of 80% of clozapine. These results paved the way for the application of these materials to the treatment of actual waters.

Regarding the experiments performed on Leponex tablets, it is notable that the inhibitory effect is more marked with both catalysts. This is likely attributed to the substantial presence of excipients in the tablet, which can potentially compete with the drug during the degradation process.

3.4. Study of the transformation mechanism

LC-HRMS was employed to identify the transformation products formed in the presence of the two photocatalysts. Clozapine disappears completely within an hour, but it gives rise to the formation of numerous degradation by-products as summarized in Table 4. The chromatographic profiles obtained for the clozapine sample in Milli-Q water after 30 min of irradiation in the presence of CA_1 are shown in Figures S5 and S6, where the proposed structural formulae corresponding to the identified transformation products (TPs) are reported alongside. Conversely, Fig. S7 shows the chromatographic profiles with the *m/z* signals extracted from the total ion current (TIC) for the different

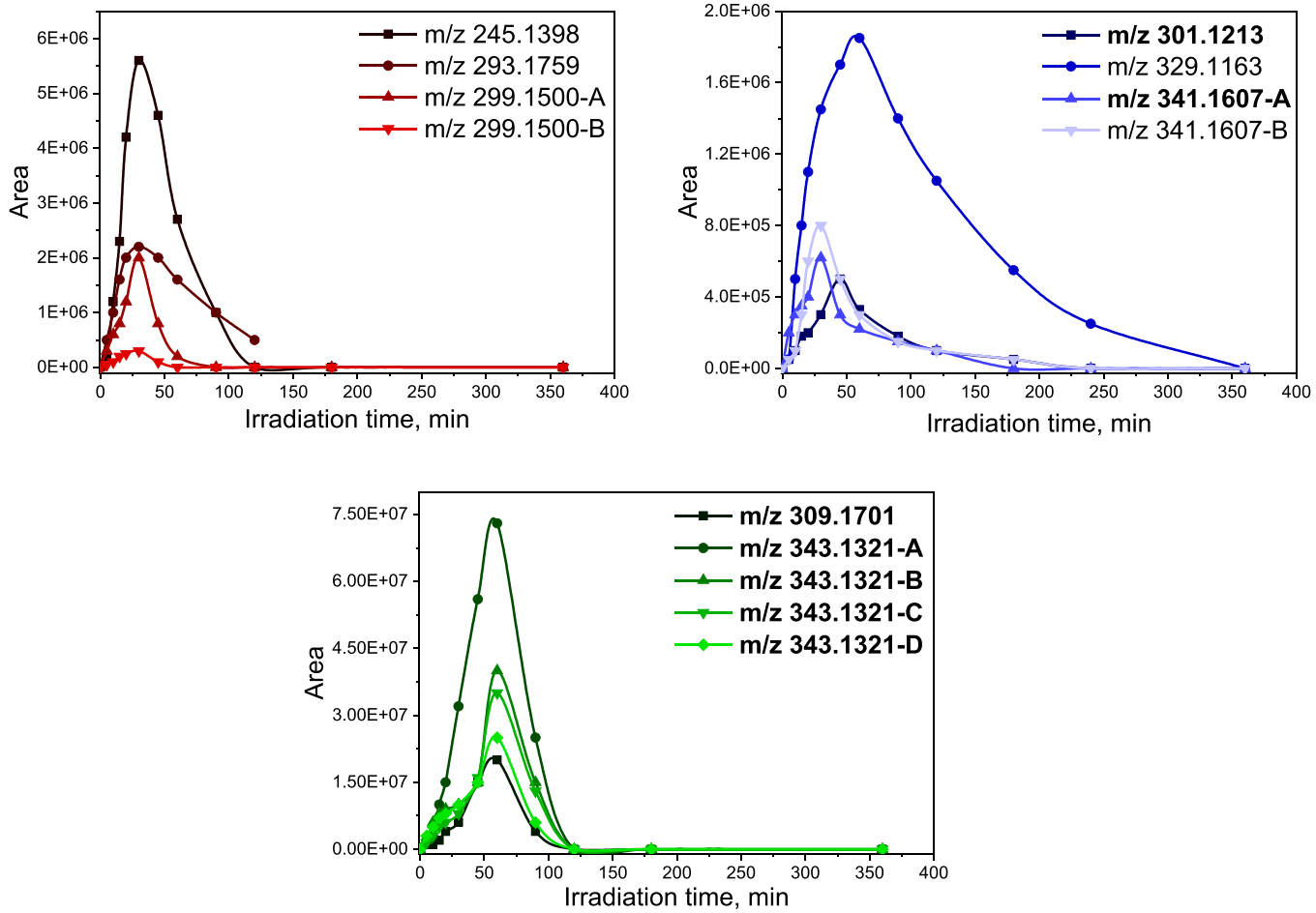

Fig. 5. Evolution of the transformation products formed during the degradation of clozapine in the presence of DEP_3:1.

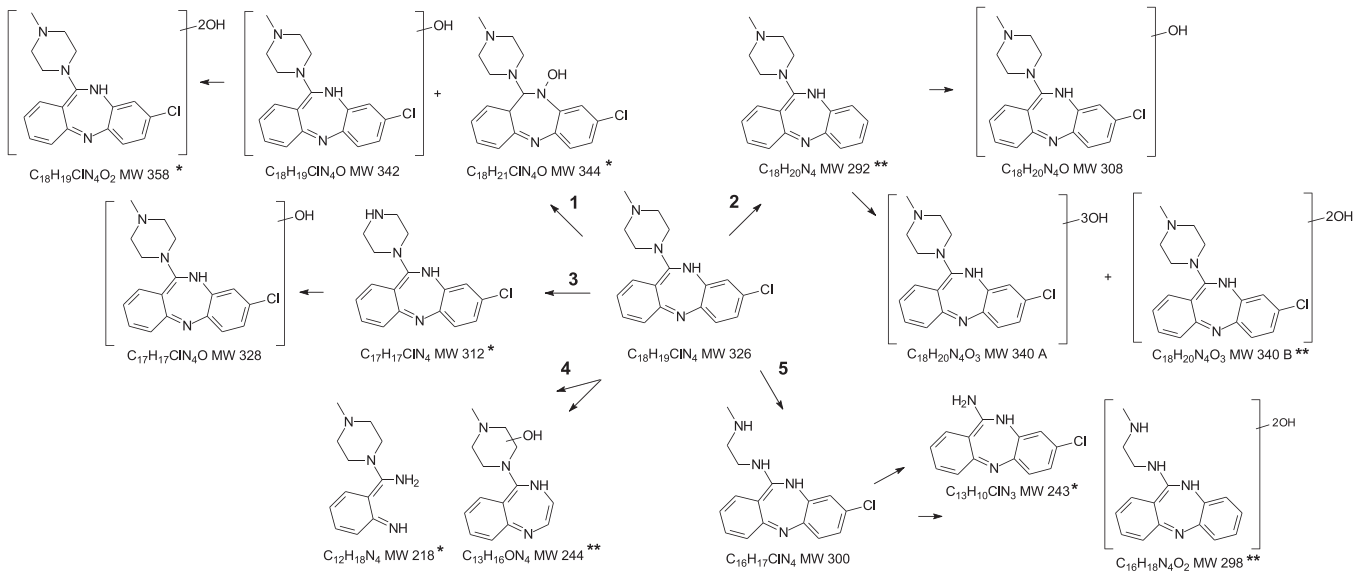

Scheme 1. Transformation pathways for the TPs formed during the photocatalytic degradation of clozapine (* species found only with CA_1; ** species found only with DEP 3:1).

degradation products formed in the presence of DEP 3:1 together with the structural formulas hypothesized for the different intermediates based on their accurate mass and on MS^n studies obtained for clozapine sample after 30 min of irradiation in MilliQ water; analogously, Figure S8 and S9 show the chromatograms obtained in River water.

All the transformation products were characterized *via* MS^2 and MS^3 spectra analyses and their spectra and fragmentation pathways are conveyed in Tables S4-S15 and Figures S11-S19. The mass accuracy of the recorded ions (*versus* calculated) was ± 0.001 u (without internal calibration). For structural elucidation of TPs structure, Xcalibur 4.0 software (version 4.0.27.13, Thermo Scientific) was used based on mass accuracy (<5 ppm) and RDB (ring double bond) index. Accurate *m/z* values and isotopic abundance in the full mass scan chromatogram were used to identify elemental composition, while MS^n fragmentation was used to hypothesize structural modifications. We followed the Shymanski rules [36] to assign the identification level 3 for the recognized TPs.

Nineteen (19) TPs were identified, some of them in the form of multiple isobaric species and 8 of them are recognized here for the first time; their kinetics of formation, relative yield and number of isomeric species detected depend on the catalyst and/or matrix used.

The evolution profiles of TPs over time in Milli-Q water are collected in Fig. 5 and S20, where it can be perceived the complete abatement for almost all intermediates within 240 min. of irradiation, with the only exception of TPs at 341.1607 *m/z* in the case of CA_1.

In Po River water, the degradation products follow a bell-shaped trend with the total abatement achieved within 6 hours of irradiation, with the exception, of the species with *m/z* 341.1607, 343-B, 359-A and 359-B, for their complete disappearance was not achieved in this time window (see Fig. S21 and S22).

Both catalysts shared the formation of 4 monohydroxy clozapine isomers (*m/z* 343.1321), that occurred in all matrices; the hydroxy group is reasonably located on the aromatic ring, in agreement with previous studies [20]. The methyl piperazine ring opening occurred as well with the formation of the TP at *m/z* 301.1213, as reported previously [20].

Analysing the case in MilliQ water, clozapine also underwent joint dechlorination and hydroxylation with the formation of two monohydroxy derivatives at *m/z* 309.1701 and two tri-hydroxy isomers (341-A and 341-B) (only one in the case of CA_1).

Conversely, several other TPs were detected with only one of the two catalysts.

Considering the case of CA_1, the dihydroxylation (*m/z* 359.1275) occurs as well as the formation of the TP at *m/z* 345.1478, attributed to a mono-hydroxylated molecule, where the cleavage of the C═N bond in the central ring is involved. Furthermore, clozapine underwent the detachment of the methyl group from the 1,4-diazamethylpiperazine ring, to form the TP at *m/z* 313.1218, the methyl piperazine ring detachment (TP at *m/z* 244.0638) and the breakage of the 7 carbons ring with the loss of the chlorobenzene (*m/z* 219.1600) as observed in previous studies [20].

In the case of the DEP 3:1 catalyst, five additional TPs were detected and identified here for the first time. They involved the combined monohydroxylation and demethylation, with the formation of the TP at *m/z* 329.1163, the dechlorination of clozapine with the formation of TP at *m/z* 293.1759, the jointly loss of the chlorobenzene moiety and monohydroxylation (TP at *m/z* 299.1500), and the formation of two isomers at *m/z* 245.1398, well matched with the loss of C_2H_2Cl and the insertion of two oxygens.

The same trend in terms of types, kinetics and yield of TPs was also maintained in River water for both catalysts with only few exceptions. In the case of DEP 3:1, some secondary TPs, namely at *m/z* 245 and 341 and in the case of CA_1 TPs at *m/z* 345 and 309, were not detected, probably because they are below the detection limit.

The search for degradation products and the study of their transformation in the river matrix largely confirms what has been simulated with the experiments in Milli-Q water, so suggesting that the degradation mechanism of clozapine is slightly influenced by the organic matter dissolved in the waters of the Po River.

Considering the profile of appearance and disappearance of the identified degradation products and their hypothesized structures, the transformation of clozapine could proceed through five concomitant pathways collected in Scheme 1, which include:

1-Monohydroxylation followed by oxidation of an alcohol group to a ketone group and/or di-hydroxylation, important for both catalysts.

2-Dechlorination with the formation of (mono and tri)-hydroxylated transformation intermediates, favoured in the presence of DEP 3:1.

3-Demethylation of the 1,4-diazamethylpiperazine ring followed by hydroxylation, marked with CA_1.

4-Detachment of the chlorobenzene ring, favoured with CA_1.

5-1,4-Diazamethylpiperazine ring opening, followed by side-chain removal and/or dechlorination and hydroxylation.

Table 5
Toxicity predictions for clozapine and its transformation products using ECOSAR software.

$[M + H^+]$	Empirical formula	Acute toxicity [mg/L]			Chronic toxicity (ChV) [mg/L]		
		Fish (LC_{50})	Daphid (LC_{50})	Algae (EC_{50})	Fish	Daphid	Algae
327.1374 (clozapine)	$C_{18}H_{20}N_4Cl$	17.7	2.32	1.58	0.764	0.210	0.563
219.1600	$C_{12}H_{19}N_4$	749	71.5	91.5	85.7	4.74	25.9
244.0638	$C_{13}H_{11}N_3Cl$	6.49	4.30	6.02	0.760	0.641	2.22
245.1398	$C_{13}H_{17}ON_4$	379	38.5	43.6	36.0	2.70	12.9
293.1759	-	-	-	-	-	-	-
299.1500 A	$C_{16}H_{19}O_2N_4$	25.2	3.20	2.33	1.21	0.280	0.811
299.1500 B	$C_{16}H_{19}O_2N_4$	144	16.0	15.2	10.4	1.23	4.80
301.1213	$C_{16}H_{18}N_4Cl$	26.0	3.29	2.41	1.25	0.287	0.835
309.1701	$C_{18}H_{21}ON_4$	45.2	5.50	4.35	2.47	0.461	1.47
313.1218	$C_{17}H_{18}N_4Cl$	-	-	-	-	-	-
329.1163	$C_{17}H_{18}ON_4Cl$	23.3	2.98	2.13	1.09	0.263	0.746
341.1607 A	$C_{18}H_{21}O_3N_4$	1.53×10^3	143	191	186	9.27	53.1
341.1607 B	$C_{18}H_{21}O_3N_4$	224	24.1	24.3	17.8	1.79	7.51
343.1321 A	$C_{18}H_{20}ON_4Cl$	65.2	7.77	6.40	3.78	0.639	2.13
343.1321 B	$C_{18}H_{20}ON_4Cl$	38.3	4.76	3.62	1.97	0.407	1.24
343.1321 C	$C_{18}H_{20}ON_4Cl$	554	56.1	64.0	53.1	3.93	18.9
343.1321 D	$C_{18}H_{20}ON_4Cl$	92.4	10.7	9.32	5.82	0.860	3.04
345.1478	$C_{18}H_{22}ON_4Cl$	-	-	-	-	-	-
359.1275 A	$C_{18}H_{20}O_2N_4Cl$	41.0	5.09	3.88	2.11	0.434	1.32
359.1275 B	$C_{18}H_{20}O_2N_4Cl$	203	22.3	21.7	15.2	1.69	6.78

-(input was not found in the database).

Overall, the hydroxylation reaction is the favoured one and the 4 monohydroxylated isomers can be considered as primary transformation products. The proposed paths (1) and (2) are the most favoured, with pathway 1 more valuable in River water. The first step of pathway 3 and pathway 4 only occurs in the presence of CA_1 and is faster and more relevant in river water. As regards the path (5), the first step takes place in all cases, while demethylation and hydroxylation only occur in the presence of DEP 3:1.

3.5. *In silico evaluation of toxicity*

Multi-species assessment is crucial for toxicity evaluation during such treatments. Since the identified TPs of clozapine are not commercially available, the ECOSAR program was employed as an alternative to predict aquatic toxicity for fish, daphnia, and algae. This tool can assess and predict the acute and chronic toxicity of substances by comparing their structures to chemicals with known aquatic toxicity profiles. Consequently, it is extensively utilized for predicting toxicity of compounds encountered in water treatment procedures. Clozapine exhibited acute toxicity lower toward fish (LC_{50} 17.7 mg/L), much lower than for daphnid and green algae (2.32 and 1.58 mg/L, respectively) (Table 5). Notably, most of the TPs formed during photocatalytic treatment exhibited lower toxicity than the parent molecule. It should be mentioned that TP with *m/z* value of 341.1607 (A), displaying LC_{50} for fish up to 1.53×10^3 mg/L according to ECOSAR, is much less hazardous that the parent compound. Additionally, unidentified TPs under experimental conditions may contribute differently to the toxicity in early photocatalytic stages.

4. Conclusions

ZnO-decorated g-C_3N_4 heterogeneous catalysts were successfully synthesized. DRS UV-Vis spectroscopy reveals unique features in the mixed C_3N_4-ZnO materials, suggesting a strong cooperative effect between nitride and oxide phases. The materials exhibited negligible adsorption of clozapine, and the direct photolysis process showed minimal clozapine photolysis. The most efficient catalysts for clozapine photocatalytic degradation were identified as DEP 3:1 and CA_1. The results showed that the process followed pseudo-first order kinetics, and hydroxyl radicals are the primary reactive species in pollutant removal. Their photocatalytic performance was notably inhibited in river water and on Leponex tablets attributed to the presence of dissolved organic matter and inorganic anions and presence of excipients competing with the drug in the case of the tablets. A total of nineteen transformation products were identified, eight of which being reported herein for the first time. The key findings of this study are twofold: first, the challenging process of identifying transformation by-products can yield valuable insights into potential transformation products in aquatic environments. Second, the combination of ZnO and g-C_3N_4 exhibited strong synergistic interactions, resulting in a powerful approach to expand the range of light absorption for visible-light photocatalysts. Overall, this study provides new perspectives for the design of advanced catalysts for highly efficient photocatalytic applications.

CRediT authorship contribution statement

Sakkas Vasilios: Conceptualization, Data curation, Writing – original draft, Supervision, Writing – review & editing. **Dal Bello Federica:** Investigation, Writing – review & editing. **Medana Claudio:** Investigation, Validation, Writing – review & editing. **Chrimatopoulos Christoforos:** Investigation, Methodology. **Ingaramo Lucia:** Data curation, Investigation. **Calza Paola:** Conceptualization, Funding acquisition, Writing – original draft, Writing – review & editing. **Paganini Maria Cristina:** Data curation, Validation, Writing – original draft, Writing – review & editing.

Declaration of Competing Interest

The authors declare that they have no known competing financial interests or personal relationships that could have appeared to influence the work reported in this paper.

Data Availability

Data will be made available on request.

Acknowledgements

This Special Issue is dedicated to honor the retirement of Prof. Santiago Esplugas at the Universitat de Barcelona (UB, Spain), a key figure in the area of Catalytic Advanced Oxidation Processes. We also acknowledge funding from the European Union's Horizon 2020 Research and Innovation Programme under the MarieSkłodowska-Curie Grant Agreement No101007578 (SusWater).

Appendix A. Supporting information

Supplementary data associated with this article can be found in the online version at doi:10.1016/j.cattod.2024.114582.

References

[1] J. Trawiński, R. Skibiński, Studies on photodegradation process of psychotropic drugs: a review, Environ. Sci. Pollut. Res. 24 (2017) 1152–1199.
[2] J. Secnik, M. Eriksdotter, H. Xu, M. Annetorp, A. Rytarowski, K. Johnell, S. Hägg, D. Religa, Dementia and psychotropic medications are associated with significantly higher mortality in geriatric patients hospitalized with COVID-19: data from the StockholmGeroCovid project, Alzheimers Res. Ther. 15 (1) (2023) 5.
[3] A.S.C. Perez, J.K. Challis, X. Ji, J.P. Giesy, M. Brinkmann, Impacts of wastewater effluents and seasonal trends on levels of antipsychotic pharmaceuticals in water and sediments from two cold-region rivers, Sci. Total Environ. 851 (2022) 158247.
[4] S. Aydın, F. Bedük, A. Ulvi, M.E. Aydın, Simple and effective removal of psychiatric pharmaceuticals from wastewater treatment plant effluents by magnetite red mud nanoparticles, Sci. Total Environ. 784 (2021) 147174.
[5] C. Jiménez-Holgado, C. Chrimatopoulos, V. Stathopoulos, V. Sakkas, Investigating the utility of fabric phase sorptive extraction and hplc-uv–vis/dad to determine antidepressant drugs in environmental aqueous samples, Separations 7 (3) (2020) 1–14.
[6] P. Calza, C. Jiménez-Holgado, M. Coha, C. Chrimatopoulos, F. Dal Bello, C. Medana, V. Sakkas, Study of the photoinduced transformations of sertraline in aqueous media, Sci. Total Environ.. 756 (2021) 143805.
[7] L. Ma, J. Li, M. Liu, D. Yan, W. Shia, G. Xu, Occurrence and source analysis of selected antidepressants and their metabolites in municipal wastewater and receiving surface water, Environ. Sci. Process. Impacts 20 (7) (2018) 1020–1029.
[8] M.D. Hernando, M. Mezcua, A.R. Fernández-Alba, D. Barceló, Environmental risk assessment of pharmaceutical residues in wastewater effluents, surface waters and sediments, Talanta 69 (2) (2006) 334–342.
[9] R. Nassar, A. Trivella, S. Mokh, M. Al-Iskandarani, H. Budzinski, P. Mazellier, Photodegradation of sulfamethazine, sulfamethoxypiridazine, amitriptyline, and clomipramine drugs in aqueous media, J. Photochem. Photobiol. Chem. 336 (2017) 176–182.
[10] T. Kosjek, E. Heath, Applications of mass spectrometry to identifying pharmaceutical transformation products in water treatment, TrAC Trends Anal. Chem.. 27 (10) (2008) 807–820.
[11] A.Y.C. Lin, X.H. Wang, W.N. Lee, Phototransformation determines the fate of 5-fluorouracil and cyclophosphamide in natural surface waters, Environ. Sci. Technol.. 47 (2013) 4104–4112.
[12] M.L. Wilde, J. Menz, C. Trautwein, C. Leder, K. Kümmerer, Environmental fate and effect assessment of thioridazine and its transformation products formed by photodegradation, Environ. Pollut.. 213 (2016) 658–670.
[13] C.E. West, S.J. Rowland, Aqueous phototransformation of diazepam and related human metabolites under simulated sunlight, Environ. Sci. Technol.. 46 (9) (2012) 4749–4756.
[14] N.D.H. Khaleel, W.M.M. Mahmoud, O. Olsson, K. Kümmerer, Studying the fate of the drug Chlorprothixene and its photo transformation products in the aquatic environment: identification, assessment and priority setting by application of a combination of experiments and various in silico assessments, Water Res 149 (2019) 467–476.
[15] S. Yuan, X. Jiang, X. Xia, H. Zhang, S. Zheng, Detection, occurrence and fate of 22 psychiatric pharmaceuticals in psychiatric hospital and municipal wastewater treatment plants in Beijing, China, Chemosphere 90 (10) (2013) 2520–2525.
[16] A. Arimi, R. Dillert, G. Dräger, D.W. Bahnemann, Light-induced reactions of chlorpromazine in the presence of a heterogeneous photocatalyst: formation of a long-lasting sulfoxide, Catalysts 9 (7) (2019). Art. no. 7.
[17] F. Zheng, J.M. Queirós, P.M. Martins, R. Fernández de Luis, A. Fidalgo-Marijuan, J. L. Vilas-Vilela, S. Lanceros-Méndez, J. Reguera, Au-sensitised TiO_2 and ZnO nanoparticles for broadband pharmaceuticals photocatalytic degradation in water remediation, Colloids Surf. Physicochem. Eng. Asp. 671 (2023) 131594.
[18] L. Tang, J. Wang, C. Jia, G. Lv, G. Xu, W. Li, L. Wang, J. Zhang, M. Wu, Simulated solar driven catalytic degradation of psychiatric drug carbamazepine with binary BiVO4 heterostructures sensitized by graphene quantum dots, Appl. Catal. B Environ. 205 (2017) 587–596.
[19] I. Rapti, V. Boti, T. Albanis, I. Konstantinou, Photocatalytic degradation of psychiatric pharmaceuticals in hospital WWTP secondary effluents using g-C3N4 and g-C3N4/MoS2 catalysts in laboratory-scale pilot, Catalysts 13 (2) (2023) art.2.
[20] J. Trawiński, R. Skibiński, Rapid degradation of clozapine by heterogeneous photocatalysis. Comparison with direct photolysis, kinetics, identification of transformation products and scavenger study, Sci. Total Environ. 665 (2019) 557–567.
[21] S. Bee Abdul Hamid, S.J. Teh, C. Wei Lai, Photocatalytic water oxidation on ZnO: a review, Catalysts 7 (3) (2017) 93.
[22] H. Tanga, R. Wang, C. Zhao, Z. Chen, X. Yang, D. Bukhvalov, Z. Lin, Q. Liu, Oxamide-modified g-C3N4 nanostructures: tailoring surface topography for high-performance visible light photocatalysis, Chem. Eng. J. 374 (2019), 1064–10.
[23] G. Mamba, A.K. Mishra, Graphitic carbon nitride (g-C3N4) nanocomposites: a new and exciting generation of visible light driven photocatalysts for environmental pollution remediation, Appl. Catal. B: Environ. 198 (2016) 347–377.
[24] E. Cerrato, C. Gionco, M.C. Paganini, E. Giamello, E. Albanese, G. Pacchioni, Origin of visible light photoactivity of the 576 CeO2/ZnO heterojunction, ACS Appl. Energy Mat. 1 (2018) 4247–4260.
[25] J. Tauc, The Optical properties of Solids, Academic Press, NewYork, 1966.
[26] J. Kuang, J. Huang, B. Wang, Q. Cao, S. Deng, G. Yu, Ozonation of trimethoprim in aqueous solution: Identification of reaction products and their toxicity, Water Res. vol. 47 (8) (2013) 2863–2872, doi: 2863-2872, 10.1016/j.watres.2013.02.048.
[27] K.S. Tay, N. Madehi, Ozonation of ofloxacin in water: by-products, degradation pathway and ecotoxicity assessment, Sci. Total Environ. vol. 520 (2015) 23–31, https://doi.org/10.1016/j.scitotenv.2015.03.033.
[28] J. Wrobel, J. Piechota, On the structural stability of ZnO phases, Solid State Commun. 146 (2008) 324–329.
[29] E. Cerrato, M.C. Paganini, Mechanism of visible photon absorption: unveiling of the C3N4–ZnO photoactive interface by means of EPR spectroscopy, Mater. Adv. 1 (2020) 2357.
[30] A. Actis, F. Sacchi, C. Takidis, M.C. Paganini, E. Cerrato, Changes in structural, morphological and optical features of differently synthetized C3N4-ZnO heterostructures: an experimental approach, Inorganics 10 (2022) 119.
[31] W. Yu, D. Xu, T. Deng, Enhanced photocatalytic activity of g-C3N4 for selective CO_2 reduction to CH_3OH via facile coupling of ZnO: a Direct Z-scheme mechanism, J. Mater. Chem. A 3 (2015) 19936–19947.
[32] Pereira Cavalcante, R.Martins de Oliveira, D. de, Melo da Silva, L. Giménez, J. Esplugas, S.C.ésar de Oliveira, S.Falcao Dantas, R. Sans, C. Machulek Jr, A. Evaluation of the main active species involved in the TiO_2 photocatalytic degradation of ametryn herbicide and its by-products, J. Environ. Chem. Eng. 9 (2) (2021) 105109.
[33] J. Zhang, J. Li, H. Su, Y. Zhao, X. Zeng, M. Hu, W. Xiao, X. Mao, H-bonding effect of oxyanions enhanced photocatalytic degradation of sulfonamides by g-C3N4 in aqueous solution, J. Hazard Mater. 366 (2019) 259–267.
[34] J.Q. Liu, C.G. Li, R.J. Qu, L.H. Wang, J.F. Feng, Z.Y. Wang, Kinetics and mechanism insights into the photodegradation of hydroperfluorocarboxylic acids in aqueous solution, Chem. Eng. J. 384 (2018) 644–652.
[35] P. Calza, C. Medana, E. Padovano, V. Giancotti, C. Minero, Fate of selected pharmaceuticals in river waters, Environ. Sci. Pollut. Res 20 (4) (2013) 2262–2270.
[36] E.L. Schymanski, J. Jeon, R. Gulde, K. Fenner, M. Ruff, H.P. Singer, J. Hollender, Identifying small molecules via high resolution mass spectrometry: communicating confidence, Environ. Sci. Technol. 48 (4) (2014) 2097–2098.